geosciences

MDPI

Article

Climate-Induced Vegetation Changes Leading to Polygenetic Soil Development in NE Hungary at the MIS3/MIS 2 Transition

Sándor Gulyás [1,*], Pál Sümegi [1], Dávid Molnár [1], Peter Almond [2], Gergő Persaits [1], Elemér Pál-Molnár [1], Tünde Töröcsik [2], Mihály Molnár [3], Katalin Náfrádi [1] and Tamás Zsolt Vári [1]

[1] Department of Geology, University of Szeged, 2-6. Egyetem u., 6722 Szeged, Hungary; sumegip@gmail.com (P.S.); molnard@gmail.com (D.M.); persaitsg@gmail.com (G.P.); palm@geo.u-szeged.hu (E.P.-M.); nafradikata@gmail.com (K.N.); vari.tamas.zsolt@szte.hu (T.Z.V.)
[2] Department of Soil and Natural Sciences, Lincoln University, P.O. Box 85084, Lincoln 7647, New Zealand; peter.almond@lincoln.ac.nz (P.A.); torocsik@gmail.com (T.T.)
[3] Interact Centre, Institute for Nuclear Research, 18/C Bem tér, 4001 Debrecen, Hungary; namafia@atomki.hu
* Correspondence: gulyas.sandor@szte.hu or csigonc@gmail.com

Abstract

The transition from MIS3 interstadial to the coldest stadial of the last glacial (MIS 2) marked a rapid change in the climate. Findings of multiproxy (sedimentological, MS, geochemical (AAS, XRD), micromorphological, anthracological, phytolith and malacological) studies from a loess/paleosol sequence in northeastern Hungary highlighted the transformation of a reddish-brown fossil soil layer (cambisol) to a podzolic soil with signs of iterative wildfires during the terminal part of MIS3. According to our findings, a Scots pine (*Pinus sylvestris*) dominated open parkland emerged on the northern slopes during the second phase of MIS3 hosted by a special reddish-brown soil. Then the last phase of MIS3 was marked by the development of spruce (*Picea abies*) dominated open parkland. Results further suggest that vegetation change passed a critical threshold leading to an unusually rapid expansion of spruce (within ca. 100 yr). This rapid expansion of spruce, changing the geochemistry of the litter to a more acidic state likely caused the initiation of podzolization and the transformation of the original soil. The opening of MIS2 marked not only intensive dust accumulation but also a steady decline of arboreal elements as well, leading to the emergence of a cold tundra on top of the podosol with charcoal remains.

Keywords: polygenetic soil development; podsolization; vegetation and climate change; MIS 3/MIS 2 transition; Pleistocene; NE Hungary

Check for updates

Academic Editor: Valérie Andrieu-Ponel

Received: 8 May 2026
Revised: 22 June 2026
Accepted: 24 June 2026
Published: 26 June 2026

Copyright: © 2026 by the authors. Licensee MDPI, Basel, Switzerland. This article is an open access article distributed under the terms and conditions of the Creative Commons Attribution (CC BY) license.

1. Introduction

Understanding paleosol genesis and development under changing climatic conditions is a key issue of Quaternary research [1–4]. Soil formation is a complex process controlled by various factors such as parent material, water availability, temperature and vegetation development [3,5]. Paleosols documenting past soil formation provide us with a view into how these factors interacted [2,6–8]. Changes to soil forming-factors often lead to the transformation of original soil properties leading to the emergence of polygenetic soils. However, the types and exact order of past responses under changing climates are relatively less understood [2,3]. The transition of climatic conditions from the interstadial of MIS 3 to the coldest stadial of the last glacial (MIS2) marks a major transformation of the climate with differing regional aspects. Does climate change directly influence soil development simply by deteriorating microbial activities through decreasing temperatures, altering

water availability and changing the intensity and type of weathering through temperature and precipitation changes? Or does the transformation of the vegetation primarily control soil functioning? [2,3]. The present work aims to unravel these aspects via multiproxy sedimentological, geochemical and paleoecological analysis of a Late Pleistocene polygenetic paleosol from Tokaj, NE Hungary (Figure 1). Based on available radiocarbon dates, transformation of a cambisol into a podosol [9–13] occurred during the final stages of MIS 3 and first half of MIS 2 (ca. 28 ky cal BP) [10,14–17]. Numerous paleoclimatic and paleoecological studies implemented in the region have so far pointed to higher humidity values during MIS 3 compared to MIS 2 [9–12,15–19]. A recent study [17] presented paleotemperature and paleoprecipitation data for a stratigraphically correlative paleosol and the overlying loess unit from a near site at Tokaj Patkó quarry (Figure 1). However, all referenced works provided paleoclimate information at a much coarser resolution, i.e., at the scale of the entire paleosol and the overlying loess. The present study exclusively focuses on the polygenetic soil complex at the site of Tokaj-Csorgókút II and the time of soil transformation from a cambisol to a podosol to reveal fine-scale processes controlling pedocomplex formation (soil properties as well as humidity, vegetation changes).

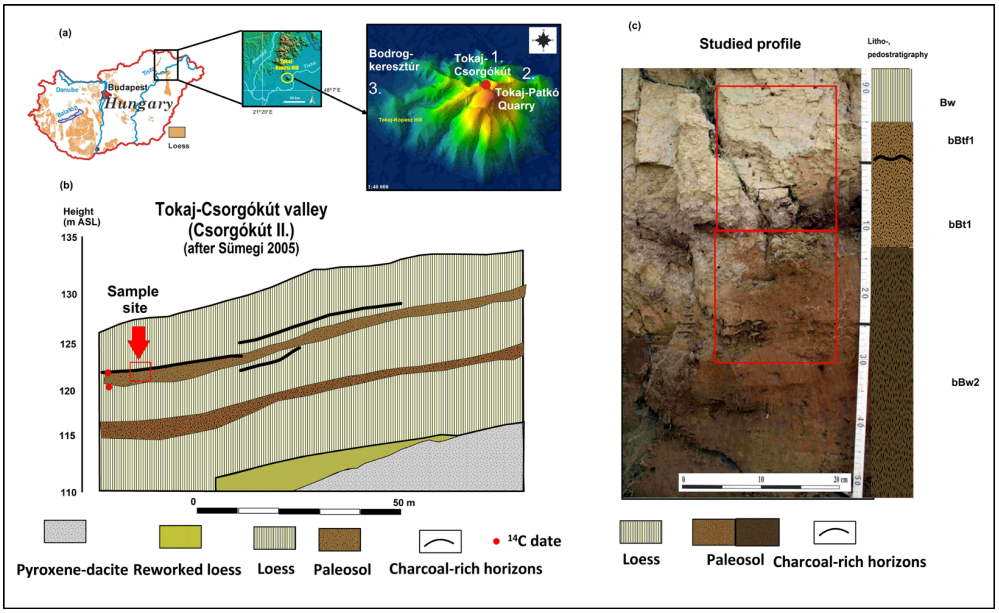

Figure 1. Location (**a**), stratigraphy of the Tokaj Csorgókút valley II profile after [10] (**b**) and the study site (**c**). The position of the original profile of [9] is also marked in addition to the new subprofile of the upper paleosol. Red squares on the photo in the right mark the position of blocks sampled.

2. Geological Setting

The study site is situated in the Csorgókút valley on the NE side of Tokaj Kopasz Hill, NE Hungary (Figure 1). The Tokaj-Csorgókút II site itself exposes a Late Pleistocene sequence along a trench with a length of ca. 50 m [9–12]. This sequence consists of three loess layers and two intercalated paleosols having an average thickness of ca. 14 m, reaching 20 m in the easternmost edge of the valley (Figure 1) [9,10]. The loess/paleosol sequence (LPS) is dated between ca. 60 ka and 17 ka [9,10,14,16] and rests above a Miocene volcanic bedrock (Figure 1). The loess embeds two dark brown paleosol horizons. The lower one probably formed between 60 and 55 ka, while the upper one was dated between 40 and 26 ka [9,10,14–17]. The upper paleosol is covered by a charcoal-bearing burnt white layer, indicating the occurrences of extensive forest fires at the end of their formation [9,10,20–22]. This paleosol is overlain by yellowish-brown loess deposited between 27 and 21 ka [10,12,15,16]. The present work focuses on the upper paleosol horizon.

As the formerly sampled profile of Sümegi [9,10] was destroyed by erosion, a new exposure was opened a couple of meters to the NE of the original (48°8′23.16″ N, 21°23′49.43″ E) (Figure 1). Here, the upper paleosol was located at a depth of 495–600 cm below the modern surface. Field observations indicate that the paleosol is a reddish brown cambisol with signs of podsolization in its upper 20 cm [10,20–22] (Figure 1). The paleosol was covered by a 10 cm-thick charcoal-bearing white layer which was interpreted to be an outcome of extensive forest fires following the cessation of pedogenesis due to emerging drier conditions [10,14,20–22]. It is overlain by yellowish-brown (10 YR 7/5) loess giving the uppermost unit of the loess/paleosol sequence.

3. Material and Methods

3.1. Sampling

The sampling focused on the transitional zone (40 cm) between the upper part of the paleosol and the overlying loess horizon also including the podzolized horizon. Two adjacent block samples have been taken with the dimensions of 20 × 20 × 20 cm (Figure 1), which was later subsampled for further analysis to overlapping blocks of 2 cm (20 samples).

3.2. Numerical Chronology

A published ^{14}C date was available from the top charcoal-bearing horizon of the upper paleosol exposed in the original profile of [9,10] which was used in our study as well [10,12,14] (Figure 1). To further constrain the age of this upper pedocomplex a single gastropod shell of autochthonous preservation from the base of the upper paleosol (bw. 590 and 600 cm) of the original profile of [9,10] was submitted for radiocarbon analysis (Figure 1). Certain herbivorous gastropods are known to yield reliable ages for dating deposits of the past 40 kyr with minimal error on the scale of perhaps a couple hundred years [14,23–27]. The preparation of the shell carbonate sample and the actual steps of the measurement followed the methods of [28–30]. Shells were ultrasonically washed and dried at room temperature. Surficial contaminations and carbonate coatings were removed by pretreatment with weak acid etching (2% HCl) before graphitization. Measurements were done in the AMS laboratory of ICER Hungarian Academy of Sciences, Debrecen, Hungary. Conventional radiocarbon ages were converted to calendar ages using the Intcal13 calibration curve [31]. Calibrated ages are reported as age ranges at the 2-sigma confidence level (95.4%). Calibrated ages bracketing the pedocomplex were compared to previously published quartz OSL and polymineral IRSL ages recorded in a corresponding stratigraphic unit at a nearby site of Tokaj-Patkó quarry (Figure 1) [15–17].

3.3. Rock Magnetism

Environmental magnetic analyses were implemented on bulk paleosol and the overlying loess samples [1,32–34]. Prior to the start of the measurement, all samples were crushed in a glass mortar. Then samples were cased in plastic boxes of 10 cm^3 and dried in air in an oven at 40 °C for 24 h. Afterwards, magnetic susceptibilities were measured at a frequency of 2 kHz using an MS2 Bartington magnetic susceptibility meter with a MS2E high-resolution sensor [35]. All of the samples were measured three times, and the average values of magnetic susceptibility are reported.

3.4. Grain-Size Distribution

Grain-size distribution was determined using the Mie method. Samples were pretreated with 1 M HCl and H_2O_2 to remove $CaCO_3$ and organic matter, respectively. For a more detailed description of the pre-treatment process, see [36]. All the samples were measured for 42 size intervals between 0.0001 and 0.5 mm using a Laser Particle Size

Analyzer type Easy Sizer 2.0 and Fritsch sieves at the Department of Geology, University of Szeged, Hungary. Grain-size classes were determined in accordance with the Wenthworth scale of grain-size distribution. However, for the clay fraction the upper boundary of 4.6 μm was considered in accordance with the general practice used in laser particle size analysis [37].

Grain-size distribution was analyzed using the indices of U-ratio defined as the ratio of 16–44 and 5.5–16 μm size classes [37], as well as the Grain Size Index (GSI) [38–40]. This is defined as the ratio of coarse silt (20–50 μm) to fine silt + clay (<20 μm). The U-ratio index ignores both the secondary formed clay minerals and the sands deposited at the site. To consider the influence of the sand fraction the fine sand/fine silt ratio was adopted [41]. Median size (MD) parameters as well as the main univariate statistical parameters of skewness and kurtosis have also been calculated. In addition, percentages of selected grain size classes of clay (<4.6 μm), coarse silt (22.6–63 μm) and sand (>63 μm) have been determined and graphed in accordance with the literature [36,38–40,42]. To assess the similarity of information recorded by the mentioned parameters and indices statistical correlations (Spearman rho) have been calculated.

3.5. Mineralogical Composition

The X-ray diffraction (XRD) measurements were carried out on a Rigaku Ultima IV XRD (x-ray: CuKα, 40 mA, 50 kV, slit: 3–60° 2Θ, interval: 0.05°, velocity of goniometer 1 o/min) at the Department of Geology of the University of Szeged. Air-dried samples were ground to 50 μm in an agate mortar before the analysis. Minerals were identified primarily by the position of their basal reflections. Specific values were used for characterization of mineral types. Semi-quantitative mineralogical composition was calculated via integral intensity calculations of areas under the diagnostic peaks. Diagrams of selected air-dried samples, where the presence of unique minerals or structures was noted, were also included.

3.6. Geochemistry

The pH of the samples was determined via potentiometry in KCl solution with an error of +/−0.2 pH units. $CaCO_3$ was measured gas volumetrically with an error of +/−10%. Total inorganic carbon content (TIC) was then calculated according to the method presented in [17]. Plasticity analysis helped determine the Arany type plasticity index (KA) (+/−3 KA units). The total organic content was determined via UV/VIS photometry. Concentration of nitrite-nitrate based nitrogen as well as sulphates in soil samples after water extraction was determined using photometric and turbidimetric methods in the Soil Laboratory of Kecskemét, Institute of Agriculture of the Hungarian Academy of Sciences.

Chemical composition of the samples for selected major and trace elements (Na, K, Ca, Mg, Fe, Mn, Sr, Ba, Al, Ti) was recorded via the flame AAS technique in a Perkin-Elmer 100 AAS spectrometer using conventional standards of known concentrations. Preparation of acid leachates followed the method presented in [43]. In addition, X-ray fluorescence was also employed to assess bulk chemistry using a Horiba wavelength dispersive spectrometer (Tube 3 kW Cr anode, 50 kV, 50 mA). Major elements (MgO, Al_2O_3, SiO_2, K_2O, CaO, Ti_2O, Fe_2O_3) were determined on fused beads of samples mixed with lithium tetraborate (ratio sample/flux 2:1). Trace elements measured were Cr, Cu, Zn, Sr, Rb, Zr. Scattered radiation was used for matrix correction [44,45]. Reproducibility is better than 2%. In the case of major elements, the accuracy of the measurements, as determined by using international standards, is 0.8–1.5 rel. % and around 5–8 rel. % for trace elements. All samples were measured twice, and the arithmetic mean was used for data analysis. Major element concentrations are expressed as wt%, volatile-free. Loss on ignition (LOI) was obtained by weighing after 10 h of calcination at 900 °C.

Simple ratios of bulk element compositions as well as chemical weathering indices are widely used to examine past weathering and pedogenesis, and to reconstruct paleoenvironmental and paleoclimatic conditions at the time of paleosol formation [46–49]. Weathering indices (WI) are usually based on the enrichment of Al and depletion of base cations (Na, K, Ca, Mg). There are multielement based Wis [50], in addition to those which focus on the weathering of the feldspar group (see [47] for a detailed review). In our work element ratios, such as Al_2O_3/SiO_2, Al_2O_3/Na_2O, K_2O/CaO, K_2O/Na_2O as well as MgO/TiO_2 were calculated [51]. The Chemical Index of Alteration was calculated by using the formula CIA = $(Al_2O_3/(Al_2O_3 + Na_2O + CaO^* + K_2O)) \times 100$; where CaO* is silicate CaO [52], as well as the Chemical Proxy of Alteration (CPA = $(Al_2O_3/(Al_2O_3 + Na_2O)) \times 100$) [47]. In addition to CPA, the index introduced by [53] was also used as these two indices factor out problems related to the calculations of feldspar bound Ca and K. The WI of Yang et al. [54] using Ti instead of Al as a refractory element specifically developed for loess/paleosol sequences was also used here. Moreover, the Ba/Sr ratio was calculated as an indicator for immobile (Ba, bound to clay)/mobile (Sr, similar behavior as Ca and mainly associated with Ca) elements (see [47] and references therein). Additionally, an A-CN-K diagram [52] plotting the concentrations of Al_2O_3, $Na_2O + CaO^*$, and K_2O was used as well to assess the type of weathering. The ratio of Ca/Sr, capturing the degree of calcification or decalcification has also been calculated [46,55,56].

3.7. Phytolith Analysis

All samples were investigated for the phytolith content. A modified version of the heavy-liquid extraction developed at the Department of Geology, University of Szeged was adopted in the analysis [57–60]. Five grams of the sample were air-dried and shaken with the addition of 10% Calgon solution to remove the organic matter and the carbonates from the sample. It was followed by the removal of the clay fraction and those with a grain size higher than 250 µm. A flotation with a heavy liquid of 2.3 g/cm^3 enabled for the separation of plant opals (phytoliths) from other non-vegetal quartz grains. The retrieved phytoliths were sorted into an Eppendorf tube in glycerine for further study. For the determination process individual slides were prepared and opals were counted line by line at a magnification of 500 X under a biological stereomicroscope type Nikon Eclipse. All identified phytolith types of the studied sample were also photographed. Altogether 200 counts were made and double-checked preceding final quantification of the results. Besides the general morphological characterization, secondary features of the identified phytoliths have also been documented following the works of [61].

3.8. Paleotemperature and Paleoprecipitation Estimations

Estimates of mean annual precipitation as well as mean annual paleotemperature were made using the formerly described weathering indices [49,62,63]. Mass-specific magnetic susceptibility (MS) has also been used [64]. These estimates used by [17] in their study enabled a comparison between the two sites. Formulas are presented in Appendix A.

4. Results

4.1. The Assumed Interval of Soil Formation

Radiocarbon dates taken from the top charcoal layer and base of the soil in the original profile of Sümegi yielded ages of 27,758 +/− 932 cal BP [10,12] and 40,007 +/− 737 cal BP (Table S1). Based on the dates an age range between c. 40 ka and ca 28 ka (i.e., the later stages of MIS 3) can be assumed for the time of deposition and soil formation.

4.2. Rock Magnetism

Magnetic susceptibility of the studied blocks ranged between 37 and 72 $\times 10^{-8}$ $m^3 \times kg^{-1}$ with an average of 46.2 $\times 10^{-8}$ $m^3 \times kg^{-1}$. The highest value (72 $\times 10^{-8}$ $m^3 \times kg^{-1}$) confined to the burnt charcoal-bearing horizon is a clear outlier in the sequence marking the transformation of magnetic minerals under extreme heat (Figure 2). Lower values between 37 and 52 are similar in range to paleosols of the LGM documented from other parts of the basin as well [18,19,26,41,65,66].

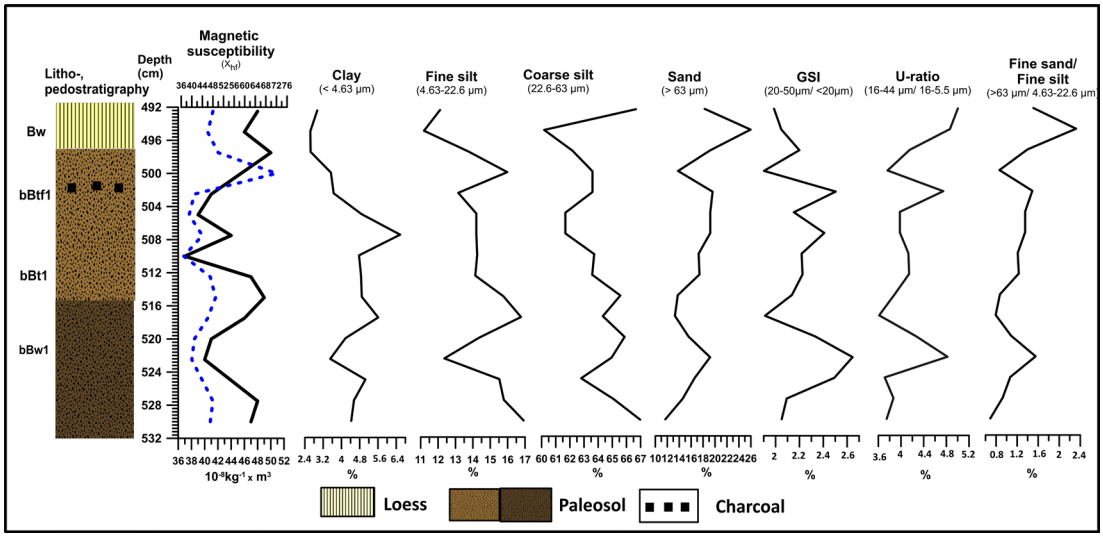

Figure 2. Mass-specific magnetic susceptibility and grain-size distribution of the studied samples.

Fluctuations in MS values display a good correlation with the clay content of the deposits. The lowest values are recorded in the eluviation zone of the podosol horizon, marking intensive leaching of organics and iron-bearing minerals. While increased values are confined to zones of clay accumulation (bBt). The transitional horizon to the overlying loess is also characterized by higher values compared to normal baseline loess values of 22–25 $\times 10^{-8}$ $m^3 \times kg^{-1}$ characteristic of the Carpathian Basin. It may be an artifact of bioturbation leading to the mixing of the horizons as seen in minor burrows in this zone.

4.3. Grain-Size Distribution

The clay content of the studied samples varies between 2.6 and 6.5% with an average of 4.3% (Figure 2). The distribution of clay is relatively even in the lower part of the sampled profile and seems to show a good correlation with magnetic susceptibility ($r^2 = 0.6$) (Figure 2). Clay is minimal in the top loess. In addition, the upper eluviation zone of the podzolized horizon (bBtf1) is also characterized by the lowest concentration of clay. All this indicates a pedogenic origin of clay. In addition, it signals a pronounced leaching and downward displacement of clay into the Bt horizon (bBt1). Coarse silt is the prominent component of the studied material giving 60–67%. There is a general upward decrease in the percentage of coarse silt. A similar pattern is noted for fine silt with ranges between 11 and 17%. The sand content varies between 12 and 25% with relatively uniform values throughout the paleosol horizon and the peak value of 25% restricted to the overlying loess horizon. GSI with values between 2 and 2.6 tends to follow an upward decrease having two peaks at the bottom of the profile and in the horizon just below the charcoal-bearing one. In contrast U-ratio (3.7–5.2) and the ratio of fine sand/fine silt (0.6–2.4) is characterized by a slight upward increase with peaks confined to the horizons, where GSI was also higher. The highest values are observed in the top loess. The mentioned trend clearly indicates an increased input of the coarser fraction towards the top of the studied profile.

4.4. Mineral Composition

The mineral composition of the paleosol samples is dominated by quartz (Figure 3 and Table S2), which is present with relatively uniform high percentage. In addition, the presence of albite, calcite, chlorite and muscovite-illite as well as kaolinite was determined. Lowest intensities of all identified minerals are observed in the overlying loess. The appearance of 27.6 o 2Θ peaks next to the albite peak of 27.93 o 2Θ in samples in the middle part of the paleosol (507.5 cm) as well as the base of the profile (527.5–530 cm), refers to the presence of microcline (Figure 4). Among clay minerals, kaolinite and muscovite/illite are always dominant in all samples.

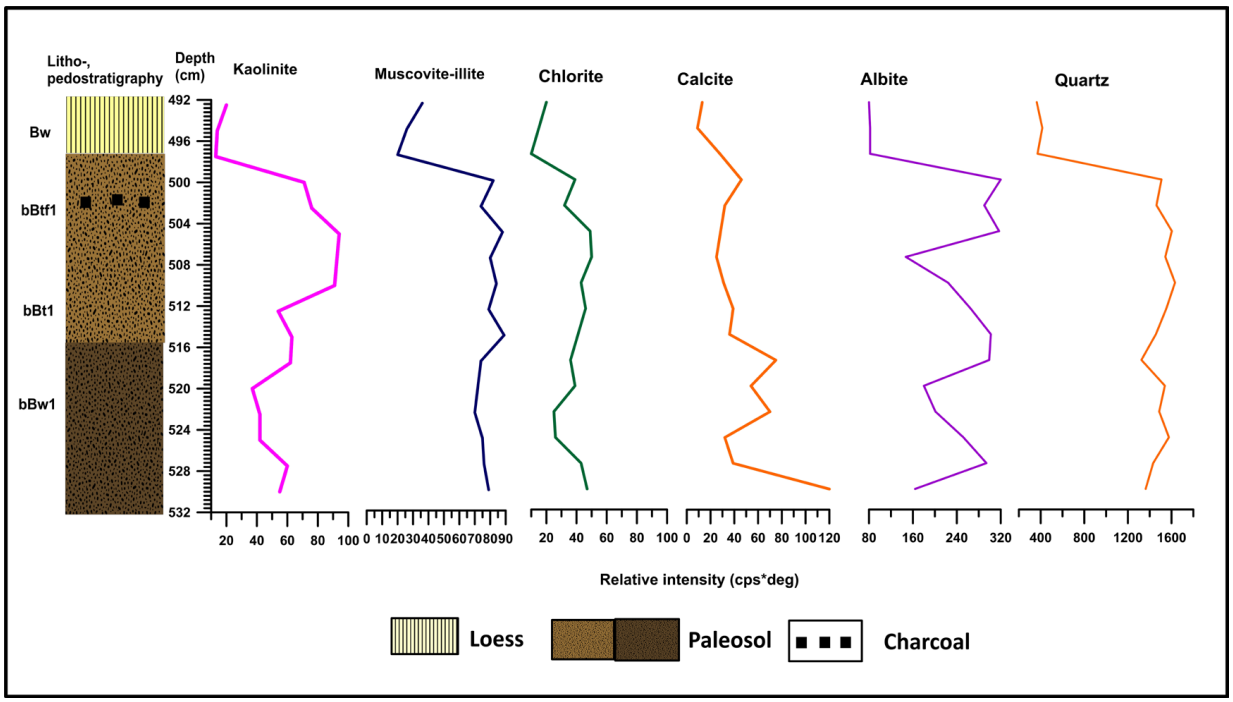

Figure 3. Semi-quantitative mineralogical composition of the studied samples.

A difference can be found in the relative abundance of kaolinite between the upper and lower part of the studied paleosol complex (Figure 3). The lowermost part is characterized by lower amounts of kaolinite. Within the upper part there is a marked increase in the intensities of kaolinite in the bBt1 horizon compared to that of the bBtf1 horizon. The widening of the kaolinite peak (25.16) in the bBt1 horizon is a clear indication of the presence of mixed structured clay minerals with higher intensities present in the lower part (Figure 5). These minerals develop via the leaching and degradation of precursor illite or smectite during pedogenesis. There is an upward decrease in the intensities of calcite reaching a minimum in the loess (Bw) covering the studied pedocomplex (Figure 3). A minor peak at a depth of 5 m indicates the accumulation of carbonates in the upper member that were leached from the overlying loess horizon. Peak intensities are noted in the uppermost part of the lower member (bBw1) reflecting leaching and downward movement of calcite from the bBtf1 unit of the upper member (Figure 3).

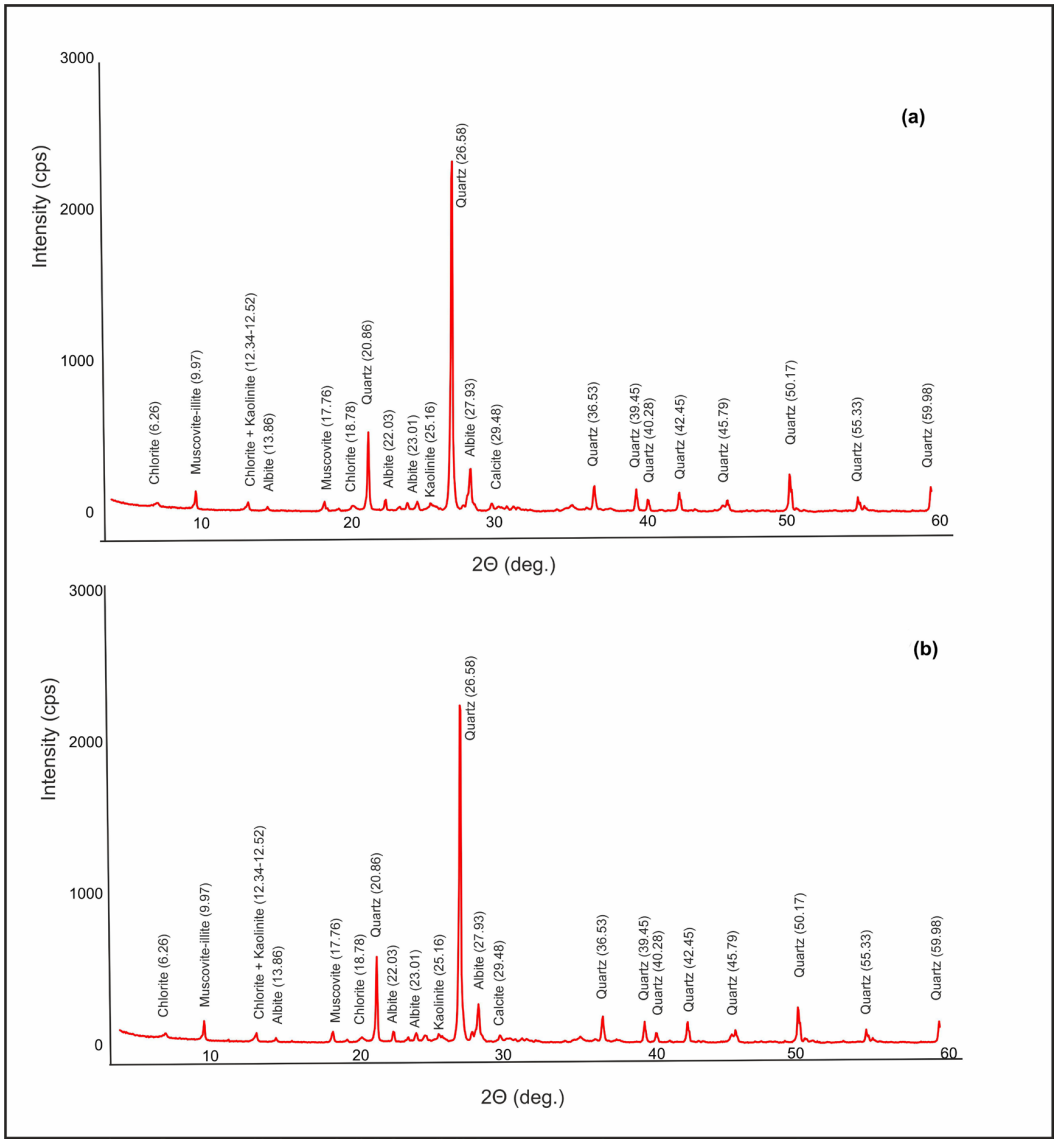

Figure 4. Typical XRD patterns of selected samples from the Bt horizon of the upper podsolic horizon.

4.5. Geochemistry

The pH is mildly basic in the topmost loess horizon (7.5–7.6) (Figure 6). Concentrations of calcium carbonate (3.6%), nitrates (7.8%) and sulphates (7.5%) are at their maxima here as well. The humic content is close to the overall minimum displaying a downward increase towards the transitional zone to the underlying pedocomplex, while the former percentages of carbonate, sulphate, nitrate undergo a rapid then gradual downward decrease. There is a major drop in the pH to ca. 6.9–7.1 in the uppermost part of the upper member of the pedocomplex corresponding to the zone of eluviation. Downwards from the zone of illuviation of the upper paleosol member the pH goes back to its average value of 7.5. The humic content is generally low in the entire studied profile (1–2%) apart from a peak value (7%) corresponding to the burnt, charcoal-rich horizon. Once this outlying value is filtered out, a generally downward increasing trend can be noted with peak values recorded in the lowermost part of the lower dark brown paleosol member marking an accumulation of organics in this horizon as a result of podsolization induced leaching in the upper member. Plasticity is the lowest in the top loess while somewhat higher values characterized the underlying pedocomplex. Highest values above 40 correspond to the burnt white horizon of the upper soil member.

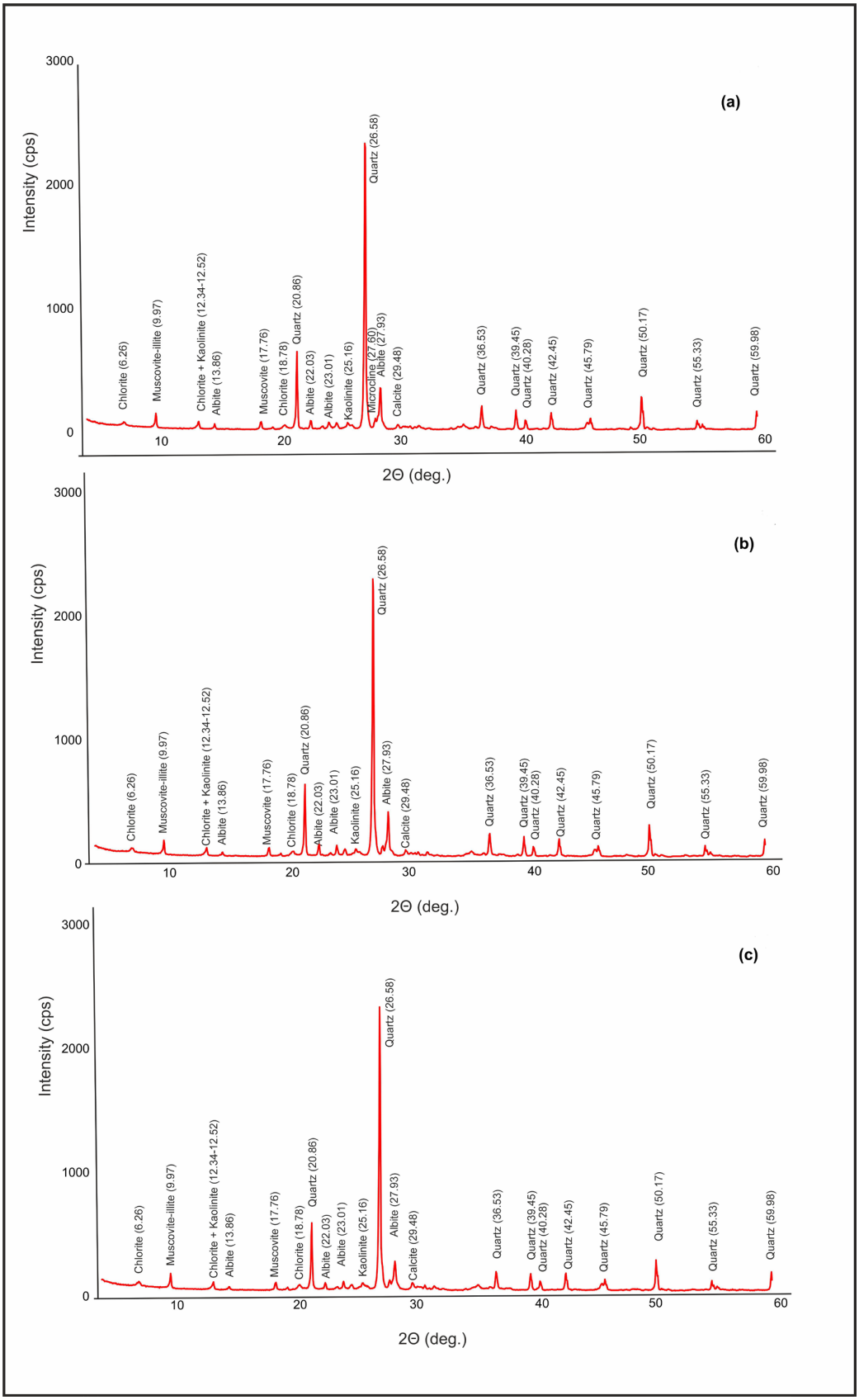

Figure 5. Typical XRD patterns of selected samples from the Bt horizons of the upper paleosol horizon (**a**) and the Bw horizon of the lower paleosol unit (**b**,**c**).

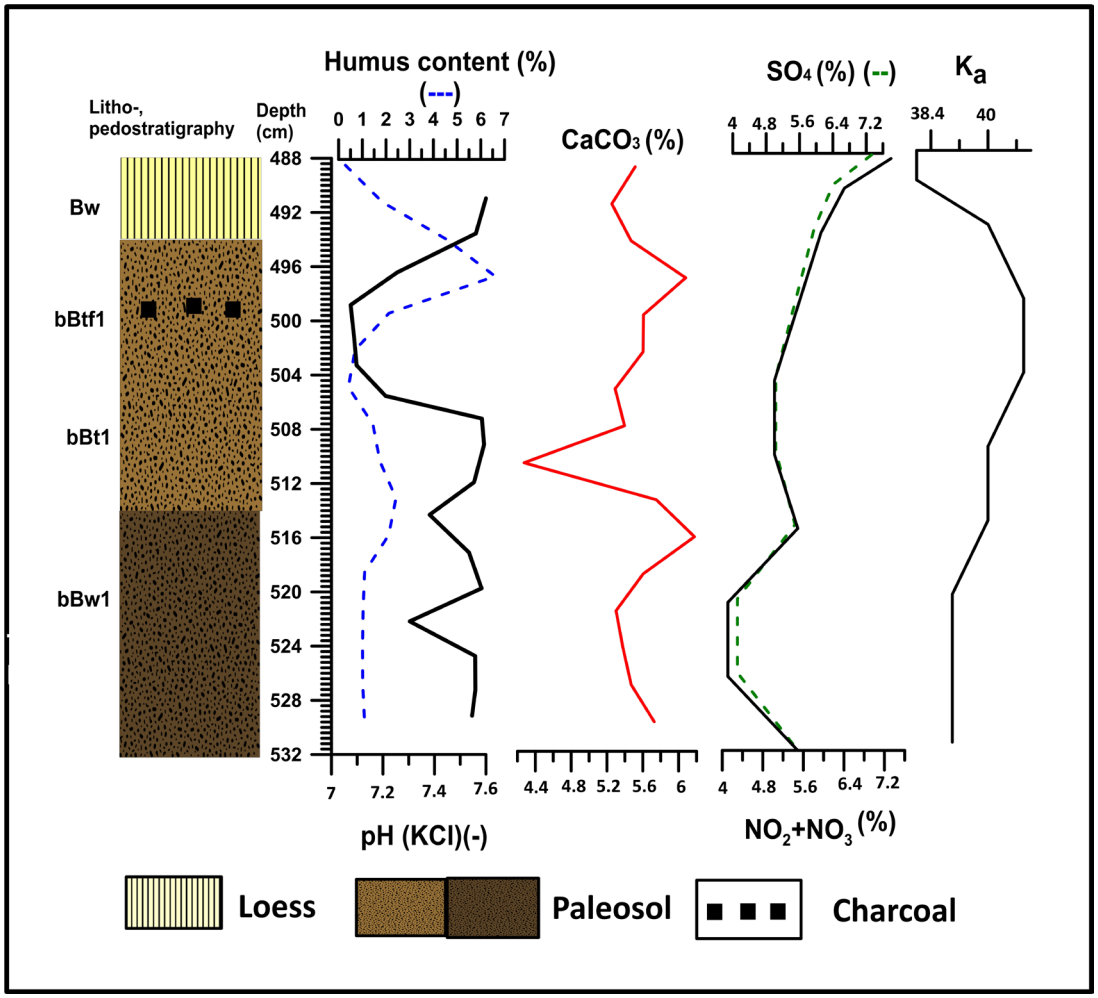

Figure 6. pH, humus, carbonate, phosphate, nitrate, sulphate content of the studied samples.

The carbonate content is generally low (Figure 6) ranging between 4.2% and 6% in the paleosol and slightly lower values of 5.2–5.6% in the overlying loess. There is a gradual downward decrease in the carbonate content with the lowest values recorded in the upper podzolized member between the depths of 500 and 513 cm indicating leaching. The highest values are confined to the directly underlying horizon marking the accumulation of carbonate here after downward displacement due to podzolization. Concentrations of sulfates and nitrates display a downward decreasing trend. The highest values of plasticity are confined to the upper podzolized horizon of the studied paleosol (Figure 6).

Loss on ignition (LOI) ranges from 4.27% to 6.18% with an average of 5.49% (Table S3). Only slightly higher values were noted for the uppermost loess and underlying upper paleosol samples from Tokaj Patkó quarry (6.56 and 6.25%, respectively) [17].

The dominant mineral is quartz throughout the profile as was seen in the previous section, which is the main source of Si in the sediment (48–51%) (Figure 7, Table S3). Highest values of SiO_2 are confined to the Bt horizon of the upper soil member (510–513 cm) indicating a leaching and downward displacement of silica as a result of podsolization from the overlying eluviation horizon (500–508 cm). The SiO_2 content is much lower compared to the data presented for loess and the underlying paleosol by [17] for the Tokaj Patkó quarry site; 73.08% and 74.31%, respectively, most likely as a result of silica leaching due to the podzolization.

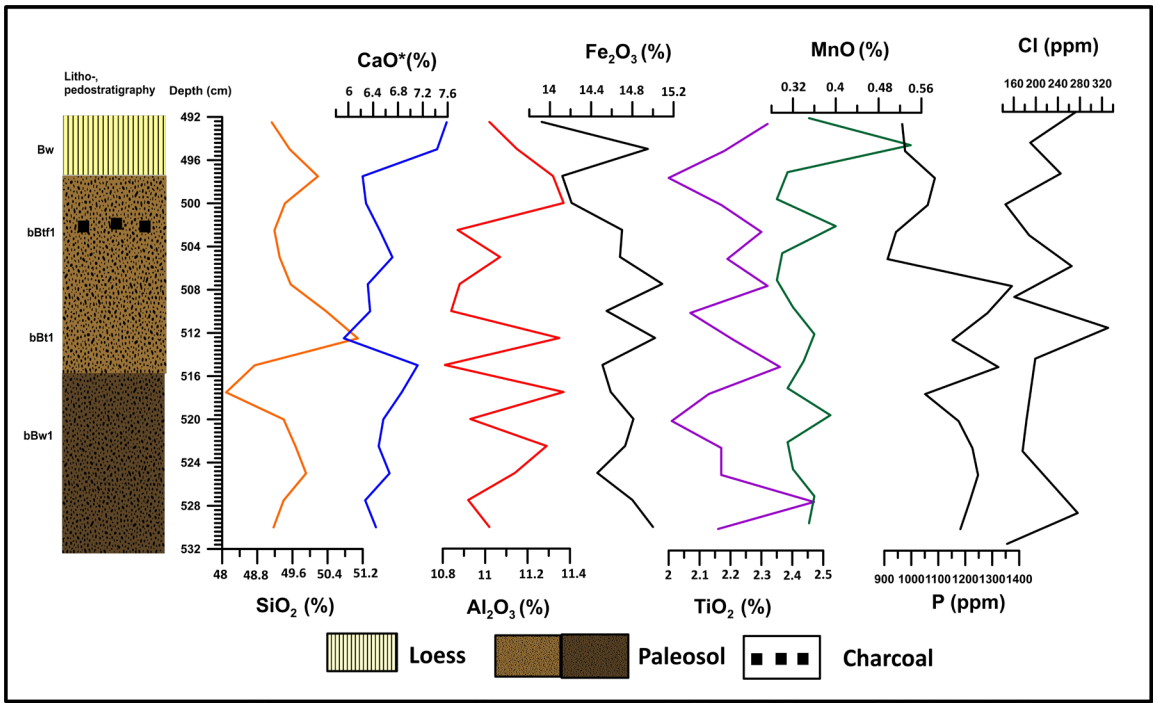

Figure 7. Bulk geochemical composition of the studied samples (all components are expressed as wt%).

The Al_2O_3 content has a very narrow range (10.81–11.37%) with an average of 11.08% (Figure 7, Table S3), which is lower than the one recorded in the nearby Bodrogkeresztúr loess/paleosol sequence (bw. 10–18%) [18,19], but comparable to the results from Tokaj Patkó quarry (11.92% for loess, 12.88% for paleosol, respectively) [17]. Values are generally higher in the upper 10 cm representing the transition from the upper member into loess. The lowest values of ca. 10.8% are confined to the upper eluviation zone of the upper paleosol member marking intensive leaching of this component too similarly to SiO_2. The corrected CaO* varies between values of 6.3 and 8.3% (Figure 7, Table S3) having an average of 7.5%, which is much higher than those recorded for paleosols in the nearby site of Bodrogkeresztúr [18,19] or Tokaj Patkó quarry [17]. CaO has a strong, negative statistically significant correlation with SiO_2 ($r^2 = -0.83$ $p < 0.05$). Uncorrected CaO also has a strong, statistically significant negative correlation with CaO based weathering indices such as K_2O/CaO ($r^2 = -0.67$) and CIA ($r^2 = -0.85$). This can indicate that CaO is strongly dependent on $CaCO_3$ and needs correction [46–49]. However, correlation remains strong and negative in case of CaO* as well for both indices: $r^2 = -0,66$ and $-0,78$, respectively. Nevertheless, a similarly strong statistically significant correlation of both CaO and CaO* with Rb ($r^2 = -0.5$ $p < 0.05$) points to the influence of $CaCO_3$ on CaO values as well. The highest CaO values are confined to the topping loess horizon. The upper podzolic soil member has lower values of CaO and CaO* compared to the lower member. There is another peak of CaO in the middle part of the lower soil member, corresponding to the zone where higher carbonate concentrations were noted (Figure 6) deriving from downward carbonate displacement via leaching. This further corroborates the assumption of carbonate dependent CaO values.

Fe_2O_3 content of the samples is relatively high (average of 14.6%) again compared to the 4–5% reported for the neighboring site of Tokaj Patkó quarry [17]. It increases downwards with overall minima present in the uppermost eluviation zone of the upper soil member (Figure 7, Table S3). There are two peaks in the underlying illuviation zone of the upper soil member marking the accumulation of iron in this horizon. TiO_2 is unusually

high (2–2.47%) in our samples (Figure 7, Table S3) compared to other loess/paleosol sequences from Hungary (0.8–0.9%) [18,19,26,51,65,66] as well as the nearby site of Tokaj Patkó quarry [17]. It has a weak positive correlation with CaO* (r^2 = 0.22) and Fe_2O_3 (r^2 = 0.13) and a moderate negative correlation with Al_2O_3 (r^2 = 0.41) and a weak negative with SiO_2 (r^2 = −0.25).

Samples have low Na_2O between 0.81 and 1.14% (Figure 7, Table S3) similarly to other documented SW Hungarian LPSs [18,19,51,67]. Much higher Na_2O concentrations are reported for both the upper paleosol and the overlying loess from Tokaj Patkó quarry; 1.78 and 1.87%, respectively [17].

The concentration of K_2O, however, is significantly higher (5.53–5.91%) at our site (Figure 7, Table S3), almost triple of the mentioned other LPS samples. It has a strong statistically significant positive correlation with Rb (r^2 = 0.66), which is a vicariant of potassium in silicates, Ba (r^2 = 0.56) and a moderate correlation with Sr, which is a vicariant of Ca, and Fe_2O_3 (r^2 = 0.2 and 0.25, respectively) implying a control of various K-bearing minerals (K-feldspars, muscovite, illite). Charred plant remains can also contribute to higher values of K in the sediment. MgO is generally low (1.35–1.65%) in the pedocomplex (Figure 7 and Table S3), similar in range to the Tokaj Patkó quarry site (1.29–1.66% for the paleosol and 1.66–2.09% for loess, respectively), compared to the overlying loess implying influences of pedogenic leaching [17].

MnO is generally low throughout the entire profile (0.29–0.54%) with highest values restricted to the uppermost loess (Figure 7 and Table S3). Yet these are much higher than the ones reported for Tokaj Patkó quarry (0.09–0.1%) [17]. Within the pedocomplex low values are generally confined to the leached horizons, while peaks appear in the underlying accumulation zones. A major peak was recorded in the charcoal-bearing zone as well marking the transformation of Mn. Concentrations of P is low in the zone of eluviation of the upper soil member with a major increase in the Bt horizon again marking downward displacement of this element via leaching (Figure 7 and Table S3). Concentrations of Cl are relatively high (120–260 ppm) compared to the nearby site of Bodrogkeresztúr [18,19]. It follows a highly variable pattern with minor peaks most likely representing the presence of redeposited material to the site of varying provenience rather than accumulation of tephra.

4.6. Phytolith Analysis

All samples yielded a minimum of 50 phytoliths apart from the uppermost loess horizon. Among morphotypes the elongate psilate LC types clearly reveal grasses (*Poaceae*). Several other morphotypes (trapeziform, tabular ovate, cuneiform) have also been identified from the samples, but they can equally be connected to grasses as well as coniferous trees due to a minimal difference. Phytoliths characteristic of spruce (*Picea abies*) and Scots pine (*Pinus sylvestris*) have also been noted in various abundance along the profile in addition to those of mosses inhabiting the undergrowth of coniferous woodlands.

Grasses are present continuously in our profile (Figure 8), however with lower proportions (20–30%) in the lower horizon of the pedocomplex. This part is clearly dominated by phytoliths of Scots pine (40–45%) containing elements of spruce (8–16%) indicating the presence of a mixed taiga at the time with a lush undergrowth containing mosses as well (4–16%). The dominance of Scots pine in this zone also indicates warmer and drier conditions emerging on the NE slopes of the hill. There is a gradual upward decrease in the abundance of Scots pine phytoliths accompanied by the disappearance of mosses. At the same time a parallel minor increase can be noted in the abundances of spruce marking an increase in humidity and decreasing temperatures. In the upper part of the pedocomplex at around the depths of 503 cm there is a slight increase in the abundance of grass phytoliths parallel with a drop in Scots pine phytoliths but a continuing increase in spruce phytoliths.

It was this zone where trichomes of grasses of forest steppe habitats were also recorded, marking an opening up of the previous denser woodland and the emergence of an open parkland type vegetation. This zone is again followed by an expansion of both arboreal elements and a drop-back of grasses in the topmost part of the paleosol. Grasses are peaking in the overlying loess with the complete disappearance of arboreal elements indicating the development of a treeless steppe as a result of intensified cooling. It is interesting to note that concentrations of Ba in the samples seem to show a good correlation with abundances of Scots pine and later spruce as well marking the importance of litter in Ba sourcing.

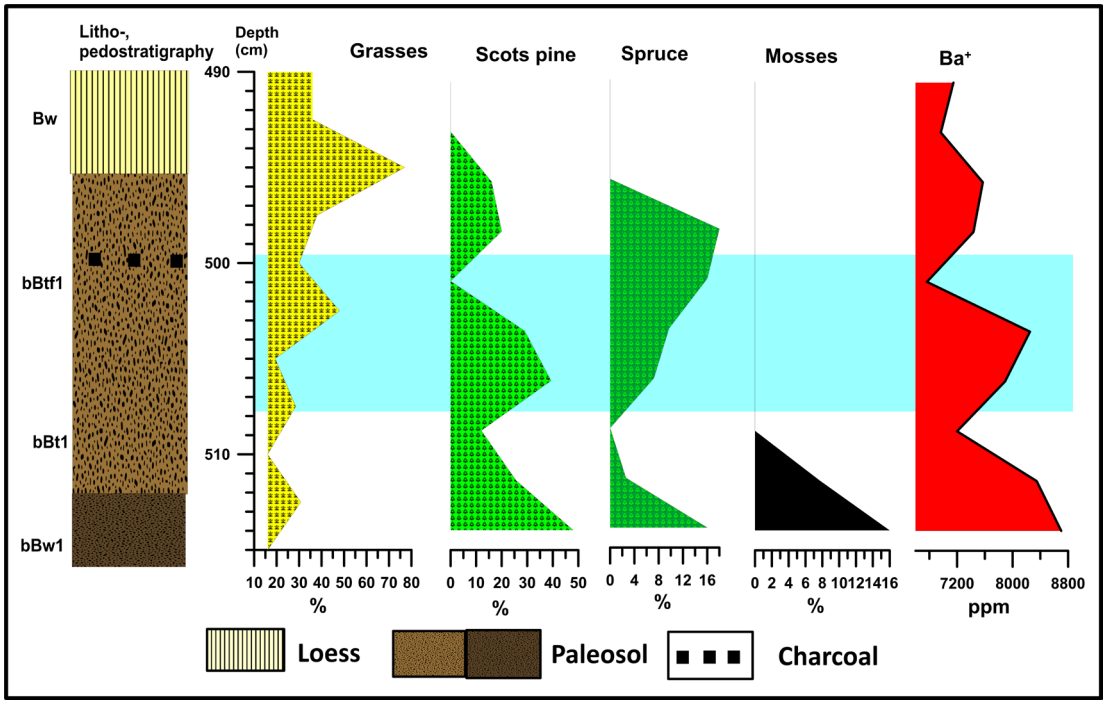

Figure 8. Abundances of identified major phytolith types and concentration changes in acid-leached Ba in the studied samples.

4.7. Paleotemperature and Precipitation Rates

Figure 9 depicts the values of reconstructed mean annual precipitation (MAP) and temperature (MAT) values using different approaches and equations (Appendix A). MAP (XRF1) ranges between 620 and 700 mm/y with the lowest values confined to the top loess. These values are somewhat lower than the ones reported for the stratigraphically corresponding paleosol (785 mm/y) and the overlying loess (697 mm/y) from Tokaj Patkó quarry. They may though be overestimated as also noted by [17]. MAP (XRF2) ranges between 510 and 555 mm/y again with lowest values confined to the loess. These are significantly lower than the ones reported by [17] for Tokaj Patkó quarry but are much closer to the current MAP rate of the area around Tokaj (546 mm/y) (1991–2000 average, Miskolc, World Data Center for Meteorology, 2011). In addition, they are also in the range given by MS based models (bw. 465–520 mm/y). MAP (XRF3) values are even lower than the ones yielded by the first two XRF and the MS-based models, ranging from 395 mm to 445 mm/y. Even lower MS-based values of 224 mm/y for loess and 325 mm/y for the paleosol were reported at the nearby site of Patkó quarry [17].

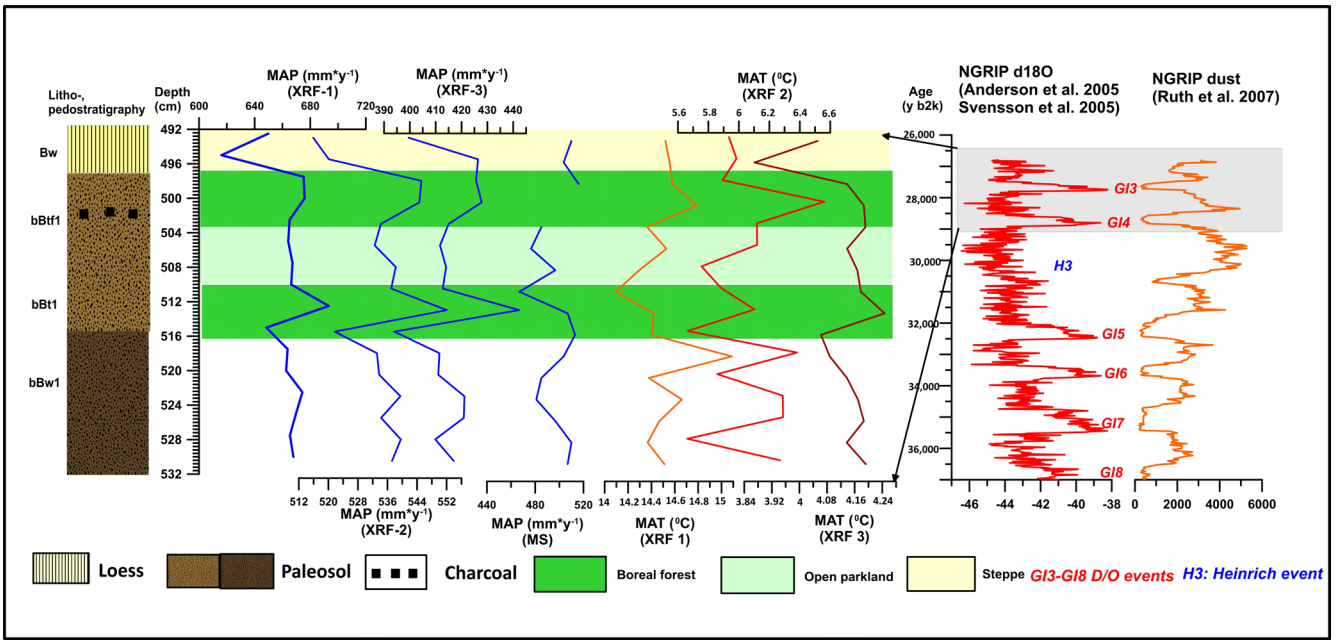

Figure 9. Reconstructed mean annual precipitation and temperature values along the profile compared to inferred vegetation changes and temperature and dust records of Greenland [68–70] for the assumed period captured by the samples of this study (ca.29-26 ka).

MAT (XRF1) values of 14.1–15.1 °C are comparable to those reported by [17] though using a different transfer function (XRF3). The other two methods yielded much lower temperatures of 5.6–6.6 °C (MAT (XRF2)) and 2.8–4.4 °C (MAT (XRF3)) compared to the first one. Both values are also lower than the ones reported by [17] for the Patkó quarry site (8.5–8.8 °C for loess and 8.9 °C and 9.9 °C for paleosol). Ref. [14] have reconstructed mean July temperatures of 12–16 °C related to topographical and aspect differences for Tokaj. Thus, mean annual temperature ranges between 6 °C and 7 °C at our site may be acceptable or somewhat low for the transitional period from MIS 3 to MIS 2. MAT at the southern Hungarian site of Katymár ranged between 7 °C and 9 °C during MIS 3/MIS 2 transition [71]. Considering the inferred 2–3 °C difference between the northern and southern Hungarian sites by [72,73] the reconstructed 6–7 °C temperature seems realistic. Looking at the temporal pattern of precipitation changes it can be clearly noted that all MAP reconstructions follow a similar trend with somewhat drier conditions in the lower unit and more humid conditions in the upper podzolic unit with a slight drop in the middle (Figure 9). The overall minimum is confined to the top loess.

5. Discussion

The reconstructed age of the studied paleosol (40 ky and 27.7 ky cal BP) is in line with published data for a stratigraphically corresponding paleosol unit located at a nearby site (Tokaj-Patkó quarry) using ^{14}C (27,683 +/− 962 y cal BP) and luminescence methods (27 +/− 2 and 39 +/− 3 ka (OSL), 30 +/− 3 and 39 +/− 4 ka (pIRIR290), 28 +/− 3 and 40 +/− 4 ka (IR50), respectively) [16]. As for grain-size distribution it is interesting to note that the charcoal-bearing horizon is characterized by an increase in the concentrations of silt compared to the underlying horizon accompanied by a minor drop in the sand content. It may hint to a larger accumulation of dust perhaps under a more open vegetation created by forest fires. However, a significant sand input either due to increased wind speed and/or erosion rates is constrained to the overlying loess. LOI shows a strong, positive statistically significant correlation with total CaO (r^2 = 0.75 $p < 0.05$) implying that it is primarily associated with carbonate minerals, but clay minerals and organic matter must have played

some role as well in the LOI budget. This pattern was noted for several Hungarian LPS as well so far [17,26,51,66,67].

Figure 10 depicts the geochemical ratios and weathering indices. The ratio of Al_2O_3 and SiO_2 is low in the upper podzolic soil horizon having higher values in the underlying soil. This is in line with the selective removal of aluminosilicates and accumulation in the underlying horizons because of podsolization. The ratios of Al_2O_3/Na_2O as well as K_2O/Na_2O are much higher in the sampled pedocomplex than the overlying loess also indicating increasing silicate dissolution. Both values are higher than the threshold (12.2 and 2) suggested by [74] corresponding to samples deposited under a moist climate. There is an upward increase in both WI-s in the profile with higher values confined to the upper podzolized horizon. K_2O/CaO displays a similar trend highlighting a more intense carbonate dissolution in the upper part. The ratio of MgO/TiO_2 is the highest in the top loess with significantly lower values in the underlying soil complex. This index is lower in the upper podzolized horizon again, referring to increased silicate dissolution.

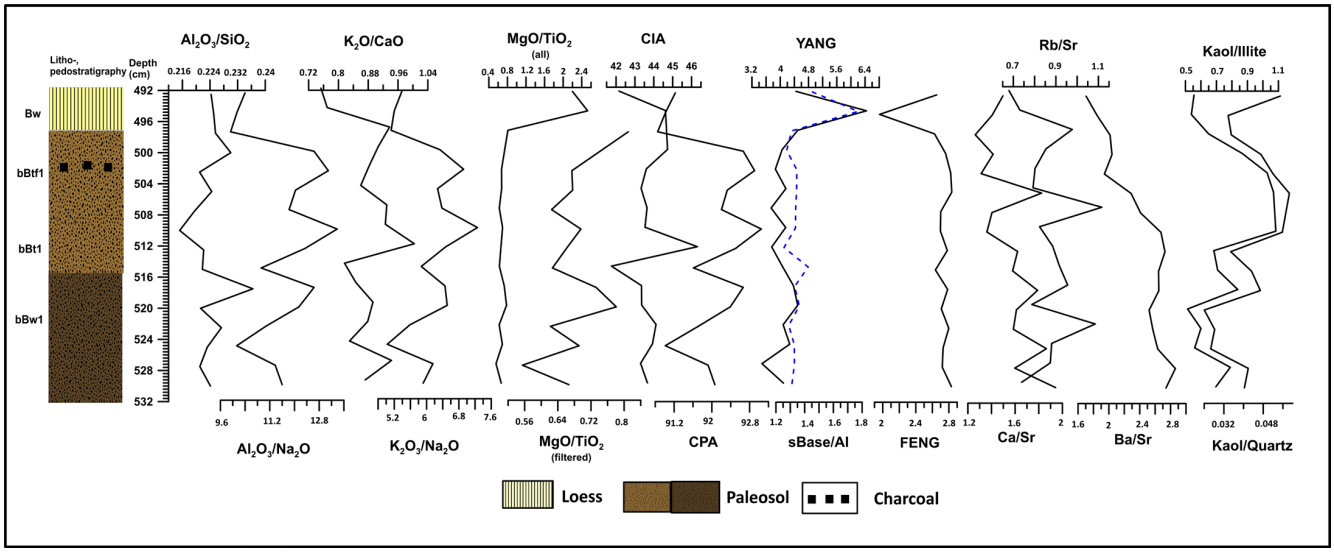

Figure 10. Changes in the intensity of various types of weathering indices used in this study.

CIA and CPA might preferentially reflect Ca and Na removal by feldspar weathering [46,47,56]. However, due to the previously mentioned carbonate dependence of Ca in our profile CPA and other Ca free indices are preferred for evaluating the degree of silicate weathering.

CIA has generally low values ranging between 42 and 47 peaking in the Bt horizon of the upper soil member. These values are lower than the ones reported for the corresponding paleosol at Tokaj Patkó quarry [17]. CIA reported from other Hungarian and Vojvodinian sites [26,46,47,51,56,66,67]is also higher compared to our site. CIA is also higher in the upper podzolized horizon seemingly hinting to increased silicate dissolution from this zone similarly to other WI. However, it is significantly influenced by increasing dust input to the site [51]. Values below 50 generally indicate the presence of unweathered Na-, Ca- and K-bearing feldspars [46,47,52,56]. Low CIA values between 54 and 56 were reported for the sand layer in the Süttő profile [56]. As there is a moderate correlation of CIA with upward increasing sand content ($r^2 = 0.32$) at our site, this factor cannot be fully ruled out either from the interpretations.

CPA is high with an average of 92 and seems to be relatively uniform with minor fluctuations in the pedocomplex. This is again higher than the average of 81 reported for Tokaj Patkó quarry [17] or any other sites from SW Hungary [26,51,66,67] or Vojvodina [47].

All this may indicate a higher rate of silicate dissolution most likely attributable to intensive podzolization in the final stage of paleosol evolution. The overall low is confined to the top loess horizon. YANG and ΣBases/Al weathering indices have generally low values in the paleosol compared to the overlying loess marking intensive weathering.

Carbonate weathering indices of Ba/Sr with an average of 2.4 as well as Rb/Sr (average of 0.86) also display an upward decreasing pattern. Low values are generally confined to the eluviation horizon.

The ratio of bulk kaolinite/illite was proposed to be another good indicator of weathering, while that of kaolinite/quartz may carry information on the degree of physical weathering [51]. Both indices seem to follow a similar trend with peak values observed in the upper podzolized horizon. This may again hint to the fact that besides intensive weathering, higher input of dust to the site seen in high CIA and sand content values towards the top may have been a factor as well in soil evolution parallelly with the intensified podzolization.

The A-CN-K ternary diagram (Figure 11) reveals the typical pattern of weathering of Ca- and Na-bearing feldspars parallel to the A-CN join in case of our samples [47,52,56,67,75]. However, our samples score closer to the CN corner than the paleosol samples of the nearby sites. The position of our samples along the A-CN joint is closer to the loess samples of Tokaj Patkó quarry [17]. This again may indicate a higher input of unweathered material to our site as stated previously in connection with the anomalously low CIA values, high CaO values and good correlation of the two with upward increasing sand content of the samples. The lower position on the A-K joint must be attributed to the intensive leaching of aluminosilicates from our sampled podzolic horizon. Along the CN-K joint, our samples are placed closer to the K corner because of much higher K_2O concentrations, again most likely attributable to intense podzolization on the one hand as well as potential contribution from the charred vegetation cover as stated before.

MIS 3 is generally agreed to have been more humid than MIS 2 in the region [10,12,19,20,72,73,76,77]. This agrees with our data and that of the nearby sites of Tokaj Patkó quarry and Bodrogkeresztúr as well [17,19]. Temperatures were higher and the relative humidity was lower in the southern Carpathian Basin, suggesting steppic, forest steppic environmental conditions and soils [13,41,65,71–73,78,79]. Ref. [80] suggested MAP values around 250–450 mm/y for SE Europe. Similar MAP values of 400 mm/y [81] and 450–850 mm/y [7] were reported for Germany as well. Taking these reports into account, MAP (XRF2, XRF3) and MAP (MS) reconstructed for our samples may seem realistic.

The recorded changes in the vegetation discussed above seem to show a good correlation with the reconstructed fluctuations of paleoprecipitation. Namely, humid periods mark the expansion of boreal arboreal elements. In the zone corresponding to the middle part of the upper podzolic soil horizon a slight drop in the precipitation rates roughly coincides with the transition into an open parkland seen from phytolith records. The final emergence of grassy vegetation, on the other hand, at the top of the profile is coeval with a marked drop in the precipitation. It is also worth noting that according to our data, the first phase of boreal forest just preceding the transition to an open parkland was characterized by higher precipitation rates than the second younger one.

Temporal changes in MAT (XRF1) and MAT (XRF2) seem to be similar, both indicating significantly cooler temperatures in the zone of the upper podzolic soil horizon compared to the lower one. Within this zone, however, there is an upward increase in the temperature from the reconstructed minimum confined to the bottom part of the podzolic soil towards the charcoal-bearing horizon with a slight drop in the middle. An opposite trend can be noted on the curve of MAT (XRF3) yielding the overall lowest temperatures of all reconstructions.

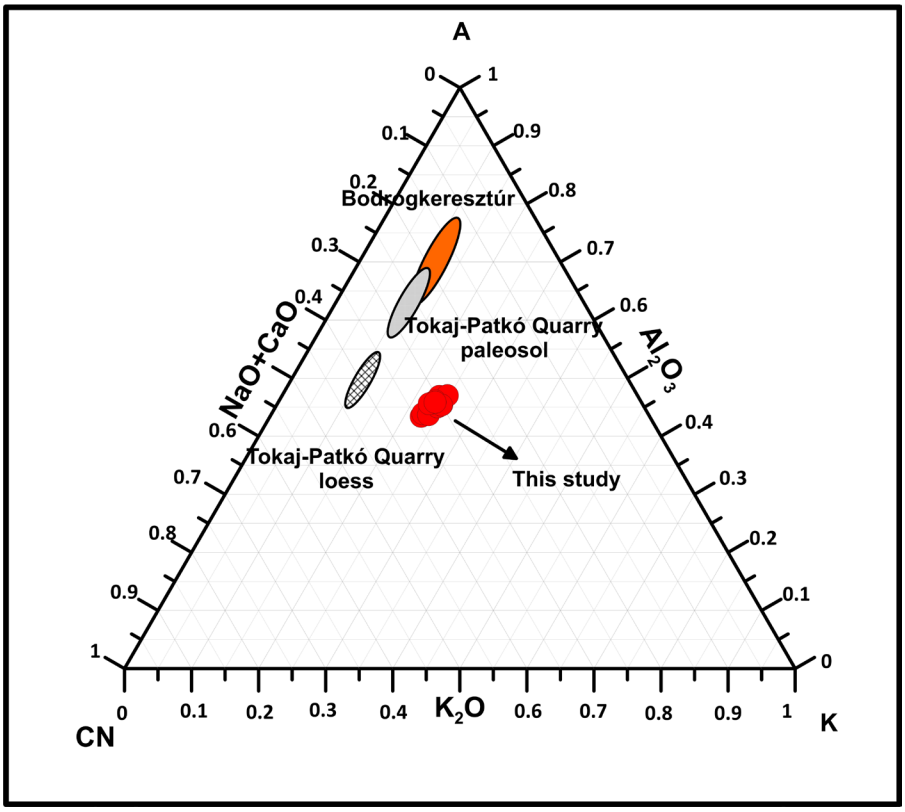

Figure 11. A-CN-K ternary plot of the studied samples displaying type of weathering. Location of samples from the nearby sites of Tokaj Patkó quarry [17] and Bodrogkeresztúr [18] is also marked for regional comparison.

The generally observed trend of change from warmer to cooler conditions between the two major paleosol units, as well as the changes in warmer to cooler and again warmer conditions in the podzolic unit (Figure 9) seem to follow the temperature changes recorded in the Greenland ice core as well (GI 4, GI3) [68–70].

Based on our findings, a Scots pine (*Pinus sylvestris*) dominated open parkland emerged on the northern slopes of Tokaj Hill during the second phase of MIS3 (ca. 37 ka) hosted by a reddish-brown soil. The last phase of MIS3 hallmarked the development of spruce (*Picea abies*) dominated open parkland. Results further suggest that the rapid expansion of spruce, changing the geochemistry of the litter to a more acidic state led to the initiation of podzolization and the transformation of the original soil. The opening of MIS2 marked not only intensive dust accumulation but also a steady decline of arboreal elements as well as the emergence of a cold tundra on top of the podzol with charcoal remains. An increase in the burnt charcoal concentrations suggests that iterative wildfires occurred in the spruce open parkland system during the last phases of MIS3. Nevertheless, the timing in increases in non-arboreal elements concomitant with declines of coniferous arboreal elements seem so rapid in our records that it almost hints to the emergence of a single event being responsible for the dramatic transition during a dry climatic phase at the beginning of MIS2. Correlative charcoal-bearing (Scots pine and birch) pale brown paleosols are present at the base of some southern Hungarian profiles at Madaras and Katymár [71–73,78,79] as well as Szeged-Öthalom (Scots pine and silver fir) [82]. A correlative forest steppe soil present at the NW Hungarian site of Basaharc was likewise rich in spruce charcoal fragments [83]. All this hints at the development of intense regional forest fires in a boreal forest steppe during the MIS3/MIS2 transition [20–22,84–87]. As seen in our records, the strong and rapid climatic fluctuations characterizing stages MIS3 and MIS2 [84–86] were

the main drivers of the observed unique vegetation and soil development changes in the analyzed region of Tokaj.

6. Concluding Remarks

Our results confirm the effects of marked and rapid climatic changes that took place on the MIS2/MIS3 transition from an interstadial to a stadial phase. The rapid expansion of spruce and decline in Scots pine at the terminal part of MIS 3 altered the litter and the soil leading to the emergence of a podosol. The succeeding increase in non-arboreal vegetation elements and a decline of coniferous vegetation happened with the emergence of dry conditions at the beginning of MIS 2. The dry phase favored forest fires in all parts of the Carpathian Basin implying a regional influence of climate change on the vegetation and paleoenvironment [77,78,84–86,88].

Supplementary Materials: The following supporting information can be downloaded at: https://www.mdpi.com/article/10.3390/geosciences16070254/s1, Table S1: new and literature chronological data for the studied pedocomplex for the site and chronological data for the corresponding stratigraphic horizon of the nearby site of Patkó quarry; Table S2: semi-quantitative mineralogical composition of the studied profile; Table S3: results of bulk geochemical analysis of the samples.

Author Contributions: S.G.: conceptualization, formal analysis, investigation, writing—original draft preparation, P.S.: methodology, funding acquisition, investigation, review and editing, D.M.: software, investigation, P.A.: validation, formal analysis, G.P.: investigation, editing, E.P.-M.: resources, data curation, T.T.: visualization, data curation, M.M.: investigation, review, K.N.: project administration, formal analysis, T.Z.V.: validation, visualization. All authors have read and agreed to the published version of the manuscript.

Funding: This research was funded by the European Union and the State of Hungary, co-financed by the European Regional Development Fund in the projects of GINOP-2.3.2-15-2016-00009 'ICER' as well as the Ministry of Human Capacities, Hungary Grant 20391-3/2018/FEKUSTRAT.

Data Availability Statement: Data is available in the supplement and upon request from the corresponding author.

Acknowledgments: We are indebted to the anonymous reviewers for their constructive comments on our work. The research was implemented within the framework of the Terra Tempus Research Group of the University of Szeged.

Conflicts of Interest: The authors declare no conflicts of interest.

Appendix A

Climate parameter
XRF-based
XRF1-MAP = −259.3ln(ÎBases/Al) + 759 [63]
XRF2-MAPa = −130.9ln(Ca/Al) + 467 [63]
XRF3-MAP = 221.1e0.0179(CIA-K) [63]
XRF1-MATb = 46.9(Al/Si) + 4 [62]
XRF2-MAT = −18.5 · [(K + Na)/Al] + 17.3 [63]
XRF3-MATc = −2.74ln(PWI) + 21.39 [88]
MS-based
MS1-MAPd = 222 + 199log(XB−C) [64]
a mollisols-specific
b inceptisol-specific
c forest soil-specific
d XB−C = [(mean MS of B horizon)−(mean MS of loess)], MS [10^{-8} m^3 kg^{-1}]

References

1. An, Z.; Kukla, G.J.; Porter, S.C.; Xiao, J. Magnetic susceptibility evidence of monsoon variation on the Loess Plateau of central China during the last 130,000 years. *Quat. Res.* **1991**, *36*, 29–36. [CrossRef]
2. Catt, J.A.; Kemp, R.; Felix-Henningsen, P.; Scholten, T. Recent and paleo-pedogenesis as tools for modelling past and future global change. *Catena* **2000**, *41*, 1–25.
3. Ponge, J.F. The soil as an ecosystem. *Biol. Fert. Soils* **2015**, *51*, 645–648. [CrossRef]
4. Powlson, D. Climatology: Will soil amplify climate change? *Nature* **2005**, *433*, 204–205. [CrossRef] [PubMed]
5. Dominati, E.; Patterson, M.; Mackay, A. A framework for classifying and quantifying the natural capital and ecosystem services of soils. *Ecol. Econ.* **2010**, *69*, 1858–1868. [CrossRef]
6. Kemp, R.A. Pedogenic modification of loess: Significance for palaeoclimatic reconstructions. *Earth-Sci. Rev.* **2001**, *54*, 145–156. [CrossRef]
7. Kühn, P.; Techmer, A.; Weidenfeller, M. Lower to middle Weichselian pedogenesis and palaeoclimate in Central Europe using combined micromorphology and geochemistry: The loess-paleosol sequence of Alsheim (Mainz Basin, Germany). *Quat. Sci. Rev.* **2013**, *75*, 43–58. [CrossRef]
8. Pietsch, D.; Kühn, P. Early Holocene paleosols at the southwestern Ramlat As-Sab'atayn desert margin: New climate proxies for southern Arabia. *Palaeogeogr. Palaeoec. Palaeocl.* **2012**, *365–366*, 154–165. [CrossRef]
9. Sümegi, P. Upper Pleistocene Evolutionary History of the Hajdúság Based on Fine Stratigraphic (Sediment, Paleontological, Geochemical) Data. Ph.D. Thesis, University of Debrecen, Debrecen, Hungary, 1989.
10. Sümegi, P. *Loess and Upper Paleolithic Environment in Hungary*; Aurea Kiadó: Nagykovácsi, Hungary, 2005; 312p.
11. Sümegi, P.; Rudner, E.; Hertelendi, E.; Borsos, S.; Deli, T.; Kozák, J.; Szöőr, G. Paleoecological research of the loess on the Kopasz mount (Tokaj, North Hungary). In *Abstract of "Geomorphology and the Changing Environment in Europe Congress"*; ELTE University Press: Budapest, Hungary, 1996; p. 112.
12. Sümegi, P.; Molnár, M.; Svingor, É.; Szántó, Z.; Hum, L.; Gulyás, S. Results of radiocarbon analysis of Upper Wechselian loess sequences from Hungary. *Radiocarbon* **2007**, *49*, 1023–1030. [CrossRef]
13. Páll, D.G.; Persaits, G.; Náfrádi, K.; Sümegi, P. Középső-würm végi fosszilis talaj- és löszréteg átmeneti szintjének komplex paleoökológiai vizsgálata a tokaji Kopasz-hegyen. *Földtani Közlöny* **2012**, *142*, 251–268.
14. Sümegi, P.; Hertelendi, E. Reconstruction of microenvironmental changes in Kopasz Hill loess area at Tokaj (Hungary) between 15.000–70.000 BP years. *Radiocarbon* **1998**, *40*, 855–863.
15. Schatz, A.K.; Zech, M.; Buggle, B.; Gulyás, S.; Hambach, U.; Markovic, S.B.; Sümegi, P.; Scholten, T. The late Quaternary loess record of Tokaj, Hungary: Reconstructing palaeoenvironment, vegetation and climate using stable C and N isotopes and biomarkers. *Quat. Int.* **2011**, *240*, 52–61. [CrossRef]
16. Schatz, A.K.; Buylaert, J.P.; Murray, A.; Stevens, T.; Scholten, T. Establishing a luminescence chronology for a palaeosol-loess profile at Tokaj (Hungary): A comparison of quartz OSL and polymineral IRSL signals. *Quat. Geochronol.* **2012**, *10*, 68–74. [CrossRef]
17. Schatz, A.K.; Scholten, T.; Kühn, P. Paleoclimate and weathering of the Tokaj (NE Hungary) loess-paleosol sequence: A comparison of geochemical weathering indices and paleoclimate parameters. *Clim. Past Discuss.* **2014**, *10*, 4069–4507.
18. Bösken, J.; Sümegi, P.; Zeeden, C.; Klasen, N.; Gulyás, S.; Lehmkuhl, F. Investigating the last glacial Gravettian site "Ságvár Lyukas Hill" (Hungary) and its paleoenvironmental and geochronological context using a multi-proxy approach. *Palaeogeogr. Palaeoclimatol. Palaeoecol.* **2018**, *509*, 77–90. [CrossRef]
19. Bösken, J.; Obrecht, I.; Zeeden, C.; Klasen, N.; Hambach, U.; Sümegi, P.; Lehmkuhl, F. High-resolution paleoclimatic proxy data from the MIS 3/MIS 2 transition recorded in northestern Hungarian loess. *Quat. Int.* **2019**, *502*, 95–107. [CrossRef]
20. Sümegi, P.; Rudner, E. In situ charcoal fragments as remains of natural wildfires of the Upper Würm in the Carpathian Basin. *Quat. Int.* **2001**, *76*, 165–176.
21. Rudner, E.; Sümegi, P. Recurring taiga forest steppe habitats in the Carpathian Basin in the Upper Weichselian. *Quat. Int.* **2001**, *76*, 177–189. [CrossRef]
22. Rudner, E.; Sümegi, P. Charcoal as a Remain of Natural and Human-set Fires of Palaeolithic Times—Case Study from Hungary. *Br. Archeol. Rep.* **2002**, *1089*, 11–18.
23. Pigati, J.S.; Quade, J.; Shanahan, T.M.; Haynes, C.V., Jr. Radiocarbon dating of minute gastropods and new constraints on the timing of spring-discharge deposits in southern Arizona, USA. *Palaeogeogr. Palaeoclim. Palaeoecol.* **2004**, *204*, 33–45. [CrossRef]
24. Pigati, J.S.; Rech, J.A.; Nekola, J.C. Radiocarbon dating of small terrestrial gastropod shells in North America. *Quat. Geochronol.* **2010**, *5*, 519–532. [CrossRef]
25. Pigati, J.S.; McGeehin, J.P.; Muhs, D.R.; Bettis, E.A., III. Radiocarbon dating late Quaternary loess deposits using small terrestrial gastropod shells. *Quat. Sci. Rev.* **2013**, *76*, 114–128. [CrossRef]

26. Újvári, G.; Molnár, M.; Novothny, Á.; Páll-Gergely, B.; Kovács, J.; Várhegyi, A. AMS 14C and OSL/IRSL dating of the Dunaszekcső loess sequence (Hungary): Chronology for 20 to 150 ka and implications for establishing reliable age-depth models for the last 40 ka. *Quat. Sci. Rev.* **2014**, *106*, 140–154.
27. Xu, B.; Gu, Z.; Han, J.; Hao, Q.; Lu, Y.; Wang, L.; Wu, N.; Peng, Y. Radiocarbon age anomalies of land snail shells in the Chinese Loess Plateau. *Quat. Geochronol.* **2011**, *6*, 383–389. [CrossRef]
28. Hertelendi, E.; Csongor, É.; Záborszky, L.; Molnár, I.; Gál, I.; Győrffy, M.; Nagy, S. Counting system for high precision C-14 dating. *Radiocarbon* **1989**, *32*, 399–408. [CrossRef]
29. Hertelendi, E.; Sümegi, P.; Szöőr, G. Geochronologic and paleoclimatic characterization of Quaternary sediments in the Great Hungarian Plain. *Radiocarbon* **1992**, *34*, 833–839. [CrossRef]
30. Molnár, M.; Janovics, R.; Major, I.; Orsovszki, J.; Gönczi, R.; Veres, M.; Leonard, A.G.; Castle, S.M.; Lange, T.E.; Wacker, L.; et al. Status Report of the New AMS 14C Sample Preparation Lab of the Hertelendi Laboratory of Environmental Studies (Debrecen, Hungary). *Radiocarbon* **2013**, *55*, 665–676. [CrossRef]
31. Reimer, P.J.; Bard, E.; Bayliss, A.; Beck, J.W.; Blackwell, P.G.; Ramsey, C.B.; Buck, C.E.; Cheng, H.; Edwards, R.L.; Friedrich, M.; et al. IntCal13 and Marine13 radiocarbon age calibration curves 0–50,000 Years cal BP. *Radiocarbon* **2013**, *55*, 1869–1887. [CrossRef]
32. Crowther, J. Potential magnetic susceptibility and fractional conversion studies of archaeological soils and sediments. *Archaeometry* **2003**, *45*, 685–701. [CrossRef]
33. Harvey, A.M.; Foster, G.; Hannam, J.; Mather, A.E. The Tabernas alluvial fan and lake system, southeast Spain: Applications of mineral magnetic and pedogenic iron oxide analyses towards clarifying the Quaternary sediment sequences. *Geomorphology* **2003**, *50*, 151–171. [CrossRef]
34. Zhou, R.; Liu, Q.; Jackson, M.J. Paleoenvironmental significance of the magnetic fabrics in Chinese loess-paleosols since the last interglacial (<130 ka). *Earth Planet. Sci. Lett.* **2004**, *221*, 55–69.
35. Dearing, J. *Environmental Magnetic Susceptibility*; Using the Bartington MS2 system; Chi Publishing: Kenilworth, UK, 1994.
36. Konert, M.; Vandenberghe, J. Comparison of laser grain size analysis with pipette and sieve analysis: A solution for the underestimation of the clay fraction. *Sedimentology* **1997**, *44*, 523–535. [CrossRef]
37. Vandenberghe, J.; Huijzer, B.; Mücher, H.; Laan, W. Short climatic oscillations in a western European loess sequence (Kesselt, Belgium). *J. Quat. Sci.* **1998**, *13*, 471–485. [CrossRef]
38. Antoine PHatté Rousseau, C.; Zöller, L.; Lang, A.; Fontugne, M.; Moine, O. Événements éoliens rapides en contexte loessique: L'exemple de la séquence du Pléniglaciaire supérieur weichselien de Nussloch (Vallée du Rhin-Allemagne). *Quaternaire* **2002**, *13*, 199–208. [CrossRef]
39. Antoine, P.; Rousseau, D.D.; Moine, O.; Kunesch, S.; Hatté, C.; Lang, A.; Zöller, L. Evidence of rapid and cyclic eolian deposition during the Last Glacial in European loess series (Loess events): The high-resolution records from Nussloch (Germany). *Quat. Sci. Rev.* **2009**, *28*, 2955–2973.
40. Antoine, P.; Rousseau, D.D.; Fuchs, M.; Hatté, C.; Marković, S.B.; Jovanovic, M.; Gaudenyi, T.; Moine, O.; Rossignol, J. High-resolution record of the last climatic cycle in the southern Carpathian Basin at Surduk (Vojvodina, Serbia). *Quat. Int.* **2009**, *198*, 19–36. [CrossRef]
41. Sümegi, P.; Gulyás, S.; Molnár, D.; Sümegi, B.P.; Törőcsik, T.; Almond, P.; Smalley, I.; Zhou, L.; Galovic, L.; Pál-Molnár, E.; et al. Periodicities of paleoclimate variations in the first high-resolution non-orbitally tuned grain size record of the past 1 ma from SW Hungary and regional, global correlations. *Aeolian Res.* **2019**, *40*, 74–90.
42. Antoine, P.; Rousseau, D.D.; Zöller, L.; Lang, A.; Munaut, A.V.; Hatté, C.; Fontugne, M. High-resolution record of the last inter-glacial–glacial cycle in the Nussloch loess-palaeosol sequences. Germany Upper Rhine Area. *Quat. Int.* **2001**, *76–77*, 211–229.
43. Dániel, P. Methods of the five-step extraction-digestion method. Results of the five-step extraction-digestion method. In *The Geohistory of Bátorliget Marshland*; Sümegi, P., Gulyás, S., Eds.; Archaeolingua Press: Budapest, Hungary, 2004; pp. 53–56+98–108.
44. DeLong, S.E.; McCullough, D.B. Compton-scattered Tungs X-ray a Measure of Mass Absorption Coefficients in Rocks. *Am. Mineral.* **1973**, *58*, 1073–1075.
45. Wilband, J.T. Rapid Method for background Corrections in trace Element Analysis by X-ray Fluorescence Analysis. *Am. Mineral.* **1975**, *60*, 320–323.
46. Bokhorst, M.P.; Beets, C.J.; Markovic, S.B.; Gerasimenko, N.P.; Matviishina, Z.N.; Frechen, M. Pedo-chemical climate proxies in Late Pleistocene Serbian-Ukrainian loess sequences. *Quat. Int.* **2009**, *191*, 111–123.
47. Buggle, B.; Glaser, B.; Hambach, U.; Gerasimenko, N.; Marković, S.B. An evaluation of geochemical weathering indices in loess–paleosol studies. *Quat. Int.* **2011**, *240*, 12–21. [CrossRef]
48. Li, C.; Yang, S. Is chemical index of alteration (CIA) a reliable proxy for chemical weathering in global drainage basins? *Am. J. Sci.* **2010**, *310*, 111–127. [CrossRef]
49. Sheldon, N.D.; Tabor, N.J. Quantitative paleoenvironmental and paleoclimatic reconstruction using paleosols. *Earth-Sci. Rev.* **2009**, *95*, 1–52. [CrossRef]
50. Retallack, G.J. *Soils of the Past*; Blackwell: Oxford, UK, 2001; p. 600p.

51. Varga, A.; Újvári, G.; Raucsik, B. Tectonic versus climatic control on the evolution of a loess–paleosol sequence at Beremend, Hungary: An integrated approach based on paleoecological, clay mineralogical, and geochemical data. *Quatern. Int.* **2011**, *240*, 71–86. [CrossRef]
52. Nesbitt, H.W.; Young, G.M. Formation and diagenesis of weathering profiles. *J. Geol.* **1989**, *97*, 129–147. [CrossRef]
53. Feng, Z.D. Geochemical characteristics of a loess-soil sequence in central Kansas. *Soil Sci. Soc. Am. J.* **1997**, *61*, 534–541.
54. Yang, S.; Ding, F.; Ding, Z. Pleistocene chemical weathering history of Asian arid and semi-arid regions recorded in loess deposits of China and Tajikistan. *Geochim. Cosmochim. Acta* **2006**, *70*, 1695–1709. [CrossRef]
55. Profe, J.; Zolitschka, B.; Schirmer, W.; Frechen, M.; Ohlendorf, C. Geochemistry unravels MIS 3/2 paleoenvironmental dynamics at the loess/paleosol sequence Schwalbenberg II, Germany. *Palaeogeogr. Palaeoclimatol. Palaeoecol.* **2016**, *459*, 537–551. [CrossRef]
56. Profe, J.; Neumann, L.; Novothny, Á.; Barta, G.; Rolf, C.; Frechen, M.; Ohlendorf, C.; Zolitschka, B. Paleoenvironmental conditions and sedimentation dynamics in Central Europe inferred from geochemical data of the loess-paleosol sequence at Süttő (Hungary). *Quat. Sci. Rev.* **2018**, *196*, 21–37. [CrossRef]
57. Persaits, G. A Fitolitok Szerepe a Geo-Archeológiai Minták Értékelésében. Ph.D. Thesis, University of Szeged, Szeged, Hungary, 2010.
58. Persaits, G.; Sümegi, P. A fitolitok szerepe a régészeti geológiai és környezettörténeti minták értékelésében. In *Geoszférák 2010*; Unger, J., Pál-Molnár, E., Eds.; GeoLitera: Szeged, Hungary, 2011; pp. 307–354.
59. Persaits, G.; Gulyás, S.; Náfrádi, K.; Sümegi, P.; Szalontay, C. Phytolithic aided paleoenvironmental studies from the Dutch Neolithic. *Open Geosci.* **2015**, *1*, 732–741.
60. Piperno, D.R. *Phytoliths: A Comprehensive Guide for Archaeologists and Paleoecologists*; Altamira Press: Oxford, UK, 2006; p. 238p.
61. Golyeva, A.A. Biomorphic analysis as a part of soil morphological investigations. *Catena* **2001**, *43*, 217–230. [CrossRef]
62. Sheldon, N.D. Quaternary glacial-interglacial climate cycles in Hawaii. *J. Geol.* **2006**, *114*, 367–376. [CrossRef]
63. Sheldon, N.D.; Retallack, G.J.; Tanaka, S. Geochemical climofunctions from North American soils and application to Paleosols across the Eocene–Oligocene boundary in Oregon. *J. Geol.* **2002**, *110*, 687–696. [CrossRef] [PubMed]
64. Maher, B.A.; Thompson, R.; Zhou, L.-P. Spatial and temporal re constructions of changes in the Asian palaeomonsoon: A new mineral magnetic approach. *Earth Planet. Sci. Lett.* **1994**, *125*, 462–471.
65. Marković, S.B.; Stevens, T.; Kukla, G.J.; Hambach, U.; Fitzsimmons, K.E.; Gibbard, P.; Buggle, B.; Zech, M.; Guo, Z.; Hao, Q.; et al. Danube loess stratigraphy—Towards a pan-European loess stratigraphic model. *Earth-Sci. Rev.* **2015**, *148*, 228–258. [CrossRef]
66. Újvári, G.; Varga, A.; Raucsik, B.; Kovács, J. The Paks loess-paleosol sequence: A record of chemical weathering and provenance for the last 800 ka in the mid-Carpathian Basin. *Quat. Int.* **2014**, *319*, 22–37. [CrossRef]
67. Újvári, G.; Varga, A.; Balogh-Brunstad, Z. Origin, weathering, and geochemical composition of loess in southwestern Hungary. *Quat. Res.* **2008**, *69*, 421–437. [CrossRef]
68. Andersen, K.K.; Svensson, A.M.; Johnsen, S.J.; Rasmussen, S.O.; Bigler, M.; Röthlisberger, R.; Ruth, U.; Siggaard-Andersen, M.L.; Steffensen, J.P.; Dahl-Jensen, D.; et al. The Greenland Ice Core Chronology 2005, 15–42 ka. Part 1: Constructing the time scale. *Quat. Sci. Rev.* **2005**, *25*, 3246–3257. [CrossRef]
69. Svensson, A.; Nielsen, S.W.; Kipfstuhl, S.; Johnsen, S.J.; Steffensen, J.P.; Bigler, M.; Ruth, U.; Röthlisberger, R. Visual stratigraphy of the North Greenland Ice Core Project (NorthGRIP) ice core during the last glacial period. *J. Geophys. Res.* **2005**, *110*, D02108. [CrossRef]
70. Ruth, U. Mineral dust records from Greenland ice cores. *PAGES Newsl.* **2005**, *13*, 17–18. [CrossRef]
71. Sümegi, P.; Molnár, D.; Gulyás, S.; Náfrádi, K.; Sümegi, B.P.; Törőcsik, T.; Persaits, G.; Molnár, M.; Vandenberghe, J.; Zhou, L. High-resolution proxy record of the environmental response to climatic variations during transition MIS3/MIS2 and MIS2 in Central Europe: The loess-paleosol sequence of Katymár brickyard (Hungary). *Quat. Int.* **2019**, *504*, 40–55.
72. Sümegi, P.; Persaits, G.; Gulyás, S. Woodland-grassland ecotonal shifts in environmental mosaics: Lessons learnt from the environmental history of the Carpathian Basin (central Europe) during the Holocene and the last ice age based on investigation of paleobotanical and mollusk remains. In *Ecotones between Forest and Grassland*; Myster, R.W., Ed.; Springer Press: New York, NY, USA, 2012; pp. 17–57.
73. Sümegi, P.; Gulyás, S.; Csökmei, B.; Molnár, D.; Hambach, U.; Stevens, T.; Markovic, S.B.; Almond, P.C. Climatic fluctuations inferred for the Middle and Late Pleniglacial (MIS 2) based on high-resolution (~ca. 20 y) preliminary environmental magnetic investigation of the loess section of the Madaras brickyard (Hungary). *Cent. Eur. Geol.* **2012**, *55*, 329–345. [CrossRef]
74. Tao, J.; Chen, M.-T.; Xu, S. A Holocene environmental record from the southern Yangtze River delta, eastern China. *Palaeogeogr. Palaeoclim. Palaeoecol.* **2006**, *230*, 204–229. [CrossRef]
75. Buggle, B.; Glaser, B.; Zöller, L.; Hambach, U.; Markovi'c, S.; Glaser, I.; Gerasimenko, N. Geochemical characterization and origin of Southeastern and Eastern European loesses (Serbia, Romania, Ukraine). *Quat. Sci. Rev.* **2008**, *27*, 10581075. [CrossRef]
76. Antoine, P.; Rousseau, D.G.; Degeai, J.P.; Moine, O.; Lagroix, F.; Kreutzer, S.; Fuchs, M.; Hatté, C.; Gauthier, C.; Svoboda, J.; et al. High-resolution record of the environmental response to climatic variations during the Last Interglacial–Glacial cycle in Central Europe: The loess-palaeosol sequence of Dolní Vestonice (Czech Republic). *Quat. Sci. Rev.* **2013**, *148*, 228–258.

77. Fitzsimmons, K.E.; Markovic, S.B.; Hambach, U. Pleistocene environmental dynamics recorded in the loess of the middle and lower Danube basin. *Quat. Sci. Rev.* **2012**, *41*, 104–118. [CrossRef]
78. Sümegi, P.; Gulyás, S.; Molnár, D.; Szilágyi, G.; Sümegi, B.P.; Törőcsik, T.; Molnár, M. ^{14}C dated chronology of the thickest and best resolved loess/paleosol record of the LGM from SE Hungary based on comparing the precision and accuracy of age-depth models. *Radiocarbon* **2020**, *20*, 403–417. [CrossRef]
79. Sümegi, P.; Gulyás, S.; Molnár, D.; Bozsó, G.; Fekete, I.; Makó, L.; Cseh, P.; Molnár, M.; Sümegi, B.P.; Almond, P.; et al. New chronology andextended palaeoenvironmental data to the 1975 loess profile of Madaras brickyard, South Hungary. *J. Quat. Sci.* **2021**, *36*, 1364–1381.
80. Frenzel, B.; Pécsi, M.; Velichko, A.A. *Atlas of Paleoclimates and Paleoenvironments of the Northern Hemisphere, Late Pleistocene–Holocene*; Geographical Institute, Hungarian Academy of Sciences: Budapest, Hungary; Gustav Fischer Verlag: Stuttgart, Germany, 1992.
81. Hatté, C.; Guiot, J. Palaeoprecipitation reconstruction by inverse modelling using the isotopic signal of loess organic matter: Application to the Nußloch loess sequence (Rhine Valley, Germany). *Clim. Dynam.* **2005**, *25*, 315–327. [CrossRef]
82. Sümegi, P.; Náfrádi, K.; Molnár, D.; Sávai, S. Results of paleoecological studies in the loess region of Szeged-Öthalom (SE Hungary). *Quat. Int.* **2015**, *372*, 66–78. [CrossRef]
83. Sümegi, P.; Gulyás, S.; Persaits, G.; Molnár, D. The loess-paleosol sequence of Basaharc (Hungary) revisited: Mollusc-based paleoecological results for the Middle and Upper Pleistocene. *Quat. Int.* **2011**, *240*, 181–192.
84. Markovic, S.B.; Hao, Q.; Ludwig, P.; Zeeden, C.; Peric, Z.M.; Mihailovic, D.; Radovic, P.; Roksandic, M.; Lindal, J.; Krsmanovic, P.; et al. Environmental dynamics recorded at Dupljaja loess section (southeastern Carpathian Basin, northern Serbia). *Catena* **2026**, *263*, 109732.
85. Markovic, S.B.; Oches, E.A.; Peric, Z.M.; Gaudenyi, T.; Jovanovic, M.; Sipos, G.y.; Thiel, C.; Buylaert, J.; Savic, S.; McCoy, W.D.; et al. The Požarevac loess–paleosol sequence: A record of increased aridity in the south-eastern margin of the Carpathian Basin during the last 350 ka. *J. Quat. Sci.* **2021**, *36*, 1436–1447. [CrossRef]
86. Marković, S.B.; Vandenberghe, J.; Perić, Z.M.; Filyó, D.; Bartyik, T.; Radaković, M.G.; Hao, Q.; Marković, R.S.; Lukić, T.; Tomić, N.; et al. Local differentiation in the loess deposition as a function of dust source: Key study novo Orahovo loess Paleosol sequence (Vojvodina, Serbia). *Quaternary* **2023**, *6*, 23. [CrossRef]
87. Fenn, K.; Millar, I.L.; Durcan, J.A.; Thomas, D.S.G.; Banak, A.; Marković, S.B.; Veres, D.; Stevens, T. The provenance of Danubian loess. *Earth Sci. Rev.* **2022**, *226*, 103920. [CrossRef]
88. Gallagher, T.M.; Sheldon, N.D. A new paleothermometer for forest paleosols and its implications for Cenozoic climate. *Geology* **2013**, *41*, 647–650. [CrossRef]

Disclaimer/Publisher's Note: The statements, opinions and data contained in all publications are solely those of the individual author(s) and contributor(s) and not of MDPI and/or the editor(s). MDPI and/or the editor(s) disclaim responsibility for any injury to people or property resulting from any ideas, methods, instructions or products referred to in the content.